# Post-Print

This is the accepted version of:

# Non-linear spacecraft component parameters identification based on experimental results and finite element model updating

**S.O. Vismara** · **S. Ricci** · **M. Bellini** ·
**L. Trittoni**

**Abstract** The objective of the present paper is to describe a procedure to identify and modelling the non-linear behaviour of structural elements. The procedure herein applied can be divided into two main steps: the system identification and the Finite Element model updating. The application of the Restoring Force Surface method as a strategy to characterize and identify localized non-linearities has
been investigated. This method, which works in the time-domain, has been chosen because it has 'built-in' characterization capabilities, it allows a direct non-parametric identification of non-linear Single Degree of Freedom systems and it can easily deal with sine-sweep excitations. Two different application examples are reported. At first a numerical test case has been carried out to investigate the modeling techniques in the case of non-linear behavior based on the presence of a free-play in the model. The second example concerns the flap of the Intermediate eXperimental Vehicle, that successfully completed its 100-minute mission on 11 February 2015. The flap was developed under the responsibility of Thales Alenia Space Italia, the prime contractor, which provided the experimental data needed to accomplish the investigation. The procedure here presented has been applied to the results of modal testing performed on the article. Once the non-linear parameters were identified, they were used to update the Finite Element model in order to prove its capability of predicting the flap behaviour for different load levels.

**Keywords** Non-linear system identification · Restoring force surface method · Finite element model updating · Space structure

S.O. Vismara
M.Sc. Graduate at Politecnico di Milano, Department of Aerospace Science and Technology, via La Masa 34, 20156, Milan, Italy
E-mail: serena.vismara@mail.polimi.it

S. Ricci
Associate Professor at Politecnico di Milano, Department of Aerospace Science and Technology, via La Masa 34, 20156, Milan, Italy
E-mail: sergio.ricci@polimi.it

M. Bellini
Thales Alenia Space, Strada Antica di Collegno 253, 10146, Turin, Italy
E-mail: marina.bellini@thalesaleniaspace.com

L. Trittoni
Thales Alenia Space, Strada Antica di Collegno 253, 10146, Turin, Italy
E-mail: laura.trittoni@thalesaleniaspace.com

# 1 Introduction

The most popular approach to perform linear system identification is modal analysis, however, in the presence of non-linearity the principles that form the basis of modal analysis are no longer valid and it becomes necessary to apply a different strategy to detect, characterize and identify localized non-linearities.

Among the well-established methods presented in [2], there exists the Restoring Force Surface method (RFS) introduced by Masri and Caughey. A parallel approach, named Force-State Mapping technique, was developed independently by Crawley and Aubert and an application can be found in [3].

This method, which works in the time-domain, has been chosen because it has 'built-in' characterization capabilities, it allows a direct non-parametric identification of non-linear systems (in so far as Single-Degree-of-Freedom systems are considered) and it can easily deal with sine-sweep excitations, which has become a quite common type of excitation since it allows a shorter testing time compared to stepped-sine test and provides a higher excitation level compared to random excitation. However, the method is not meant to deal with Multi-Degree-of-Freedom (MDOF) structures although there have been attempts to extend it to lumped

parameter MDOF structures [4]. Another limitation of the method comes from the fact that it is not able to provide any information about the location of the non-linearity.

A comprehensive explanation of the method can be found in [4], whereas experimental applications can be found in [5] to [10].

Further details on the results presented next can be found in [1], on which this paper is based.

## 2 The Restoring Force Method

The starting point of the method is the Newton's second law of motion written in the Single-Degree-of-Freedom (SDOF) form

$$m\ddot{y} + f(y, \dot{y}) = p(t) \tag{1}$$

where $f$ is the internal restoring force which acts to return the system to equilibrium when disturbed. Since $f$ is assumed to be dependent only on displacement and velocity, it can be represented as a surface over the phase-plane. A rearrangement of Eq. (1) gives the restoring force as

$$f(y(t), \dot{y}(t)) = p(t) - m\ddot{y}(t) \tag{2}$$

If the mass $m$ and the excitation $p(t)$ are known and the acceleration $\ddot{y}$ is measured, all quantities on the right side of Eq. (2) are known, and so is $f$. If velocity and displacement are also known (from direct measure or from numerical integration), the triplet $(y_i, \dot{y}_i, f_i)$ is known at each time instant: the first two values indicate a point in the phase-plane and the third the height above that point. The visualization of the surface represents a quick way of determining the type of non-linearity involved and the determination of the functional form is straightforward.

*Data processing.* Two main ways to obtain simultaneous displacement, velocity and acceleration data at each sampling instant are available depending on what are the quantities measured during the test. The easiest approach is to measure the acceleration and estimate the other two by means of numerical integration and filtering. The second approach, instead, relies on acceleration and displacement measurements in order to retrieve the velocity by means of a discrete Kalman filter. The first approach is the one applied to both the numerical and the experimental case presented next and therefore it will be explained in the following, whereas the explanation of the second technique will be presented in Appendix A since it has not be applied in this case. However, an application on experimental data of the second approach can be found in [1].

As said, the first method relies on the use of an integration scheme to obtain estimates of the missing signals. Various methods for achieving numerical integration can be found in [11] and [12]. Due to its simplicity, the chosen integration scheme for this study is the Trapezium rule. Since it suffers from the introduction of spurious low-frequency components (as stated in [4]), the time histories resulting from the integration need to be high-pass filtered. Not to introduce any phase lags, which will destroy the simultaneity of the signals, a bidirectional filtering technique must be adopted. The effect of the bidirectional filtering (zero-phase) is clearly visible in Fig. 1.

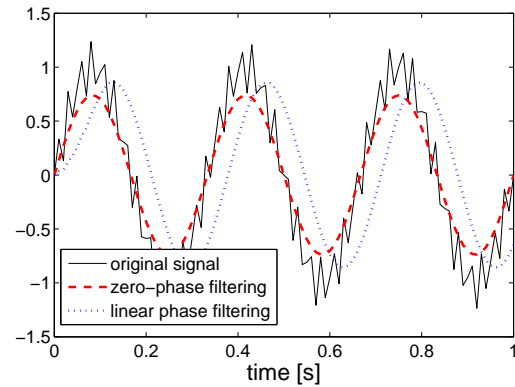A comprehensive introduction to digital filtering can be found in [13] and [14].



**Fig. 1:** Effect of zero-phase and linear phase filters on signals

## 3 Finite Element model of gaps: a simple numerical example

To predict the behaviour of non-linear systems, it is necessary to include the corresponding non-linear elements into the numerical models which describe the system. Once the non-linear parameters have been identified by means of the Restoring Force Surface method, they can be used to update the Finite Element (FE) model.

The following simulation has been carried out by means of the MSC Nastran software. Although this software is prone to be affected by convergence problems in the presence of structural non-linearities, it has been chosen because it represents the standard for both industrial an academic applications for what concern the structural analysis.

Two different approaches have been applied in order to model the gap non-linearity: the first relies on the introduction of an non-linear element which is capable of simulating a point-to-point contact for contact and friction simulations, whereas the second implies the definition of a non-linear force-deflection relationship which is treated as a di-

rect force applied locally on the structure and thus considered as an additional load in the equation of motion.

Several non-linear solution sequences are available in MSC Nastran, both in the time and frequency domain [15]. The ones taken into account for this research are the non-linear transient solution (SOL129) and the non-linear harmonic response solution (SOL128), which are both direct solution sequences. The first was chosen because, according to [15] it represents the preferred choice when non-linearities are involved, whereas the second solution sequence has been investigated because it provides results directly in the frequency domain thus allowing to directly compare them with the test results with a reduction in the time needed for post-processing. The main characteristics of these two solution sequences are shown in Table 1. In this table, the CGAP/PGAP entry refers to the first modelling approach (non-linear element) described earlier, whereas the NOLINi entry represents the second approach (non-linear load).

**Table 1:** Nastran non-linear solutions

| Nastran | Type | CGAP/PGAP | NOLINi |
|---------|------|-----------|--------|
| SOL128 | Frequency | No | Yes |
| SOL129 | Transient | Yes | Yes |

To show the set-up of these two solution sequences a plate has been modelled. The plate, shown in Fig. 2, has dimensions $0.127 \text{x} 0.0508 \text{x} 0.0012\,m$ and it is constrained at three nodes in order to resemble the constraint configuration of the IXV flap, which will be analysed at the end. The load is applied along the $z$-direction at the tip.
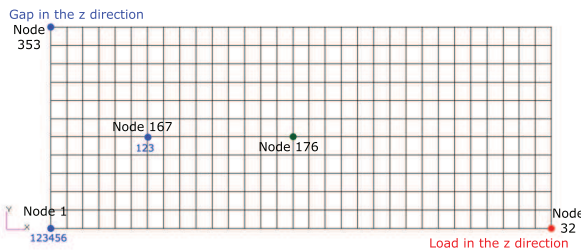


**Fig. 2:** Plate FE model

A modal analysis was run to locate the first two resonances, which were seen to occur at $79.26\,Hz$ and $304.9\,Hz$. Being the first two modes well separated, it is possible to excite the first one only so that the plate can be assumed to behave as a SDOF system.

## 3.1 Free-play modelled as element

A symmetric gap has been modelled in the $z$-direction at node 353, thus replacing the existing constraint in that direction.

The element has been modelled by means of the CGAP and PGAP Bulk Data entries which are intended, among the others, for the non-linear transient solution sequence SOL129. The PGAP entry defines the properties of the element and it is called by the CGAP entry [16].

The simulation parameters required by the aforementioned cards were chosen as follows:

– to determine the value of the axial stiffness of the closed gap, a linear spring along $z$ was introduced at node 353. The spring constant was set to $10^9\,N/m$ to simulate the constraint and a linear transient simulation was run. The results were compared to the ones obtained in the case of the actual constraint to make sure they were equal
– the same model was run with the non-linear transient solution to check the correctness of the PARAM,W4 value used to define the damping[1]
– the axial stiffness for the open gap was set to $10^{-6}\,N/m$
– the initial gap opening was chosen looking at the displacement at node 353 obtained running a simulation under sine excitation after having removed the constraint in the $z$ direction (Fig. 3). The chosen value was $4 \cdot 10^{-4}\,m$
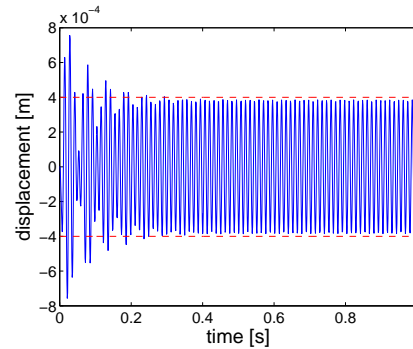


**Fig. 3:** Time response at node 353 without the $z$ constraint

The time step for the simulations was chosen taking into consideration the frequency content of the input load and the frequency of the mode of interest (the first one only). However, the SOL129 is characterized by an automatic adjustment of the incremental time, which means that the user-defined $\Delta t$ is actually used as an initial value for the time step size [15].

Two simulations were run in order to show the effects of the gap non-linearity on the plate response. The first simu-

---

[1] It is extremely important to correctly define the W4 (or W3) parameter as will be better explained in Appendix B

lation run was a linear transient solution (SOL109) with the node 353 constrained in the $z$ direction. Then the constraint was replaced by the gap modelled as explained earlier and the non-linear transient solution was run. For both analysis the input was a unit amplitude, sine sweep excitation band limited in the range $50 - 100\,Hz$ and applied at the tip (node 32) in the $z$ direction. The sweep rate was set to $4\,oct/min$, which yields a total duration of the simulation of $15\,s$. The output responses, shown in Fig. 4, were read at node 176, which is close to the Centre of Gravity (CoG).

The effect of the non-linearity can be easily spotted by the inspection of the time histories, in fact the response in Fig. 4b clearly shows the *jump phenomenon* typical of non-linear systems.
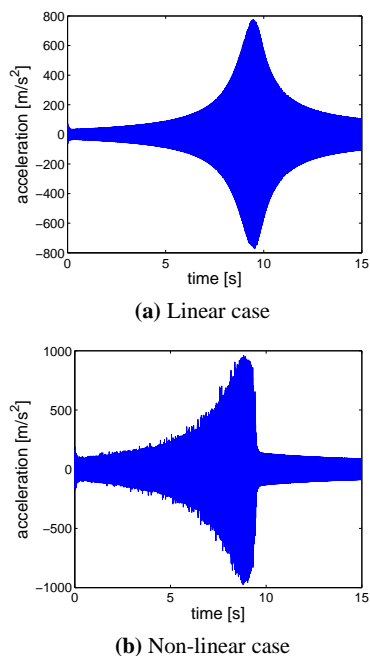


(a) Linear case



(b) Non-linear case

**Fig. 4:** Acceleration at plate CoG

## 3.2 Free-play modelled as non-linear force

As said, the Nonlinear Harmonic Response solution offers the possibility to obtain results directly comparable with the test ones, however the approach described earlier is not applicable in this case since the cards used earlier are no more available in this solution sequence. Therefore, to simulate the effects of the gap non-linearity it is necessary to introduce the NOLINi cards, which allow the definition of a non-linear force-deflection (or force-velocity) curve.

As stated in [15], the aforementioned solution sequence allows the analysis of the dynamic response of non-linear structures which exhibit a periodic response when subjected

to a harmonic excitation. This means that, to be able to describe the response as a combination of harmonic responses through the Harmonic Balance Method (which is the method implemented in this solution), the degree of non-linearity has to be light, in such a way that only a small number of sinusoids is necessary to approximate the solution.

The main issue related to this solution is convergence. Non-convergence can be due to dynamically unstable conditions, to the reaching of a bifurcation point or to an insufficient number of harmonics taken into account. In case of non-convergence, the response quantities are set to zero and the calculation continues to the next excitation frequency retaining the initial conditions of the solution from the last converged frequency.

Since the non-linearities have to mild to achieve convergence, the curve which represent the free-play non-linearity was approximated using a polynomial model of the form $p(x) = p_1 x^3$, where $p_1$ was estimated to be equal to $1.77 \cdot 10^9$ (Fig. 5). In this way it was possible to avoid the abrupt change in stiffness due to the gap closing. It has to be noted, however, that the lack of a tangent matrix due to the fact that the NOLINi Bulk Data entries define forces, not elements, could still lead to solution instabilities which will cause non-convergence.
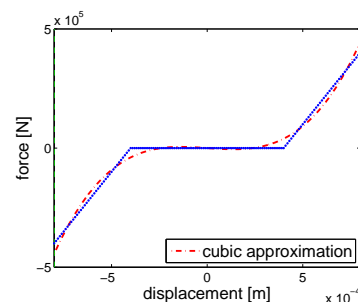


**Fig. 5:** Polynomial approximation of a symmetric gap

To define the non-linear load as a power of the displacement (or the velocity) the NOLIN3 and NOLIN4 entries [16] have been used. The NOLIN3 defines the forcing function for positive displacements, the NOLIN4 for negative displacements.

To simulate the gap, the non-linear force was applied at node 353 in the $z$ direction and the analysis was run for different load levels. The number of harmonics included in the solution is 3, because it was noted that there was no gain in increasing the number of harmonics above 3 since the solution did not improve any more. The comparison of the Frequency Response Functions (FRF) shown in Fig 6 (the so called, homogeneity test [17]) highlights the presence of the non-linearity and its effects on the natural frequency of the plate. The curve obtained for the second load level (the solid blue one) has been presented on purpose to show the effects

of non-convergence on the results, since this is a peculiarity of this solution sequence. In fact it can be seen that the response is set to zero for the frequency values in which convergence is not reached. When convergence is not reached, the calculation continues retaining the initial conditions of the solution from the last converged frequency.
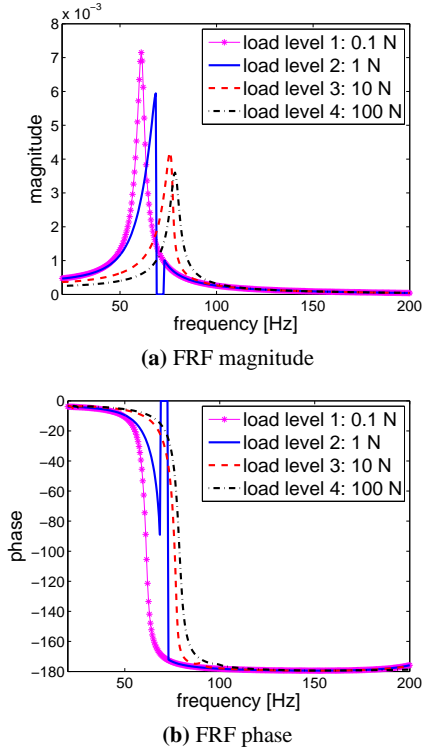


**(a)** FRF magnitude



**(b)** FRF phase

**Fig. 6:** Homogeneity test

## 4 Numerical validation of the Restoring Force Surface method

The time histories obtained in Section 3.1 can be used to validate the identification method.

Before applying the method, the simulation outputs have been resampled at a constant sampling frequency of $10\ kHz$ in order to have a better coverage of the phase-plane.

The surface and the stiffness curve resulting from the application of the Restoring Force Surface method are shown in Fig. 7. The spurious oscillations (Fig. 4b) introduced by numerical integration have the effect of producing a noisy surface. Since the stiffness curve showed a piece-wise linear trend, a non-polynomial model expressed by Eq. (3) was fitted to the numerical data and the estimated parameters were collected in Table 2 and Table 3. The exact stiffness parameters were obtained applying the identification method to the time histories obtained for two limiting cases: one with

node 353 fully constrained and one with node 353 free in the $z$-direction. The stiffness values thus obtained represent the closed and the open gap conditions in such a way that $k_-, k_+ = k_{z,constrained}$ and $k = k_{z,free}$.

$$f_s(y) = \begin{cases} k_+ y + (k - k_+)y_c & y > y_c, \\ ky & |y| \le y_c \\ k_- y + (k - k_-)y_c & y < -y_c \end{cases} \tag{3}$$
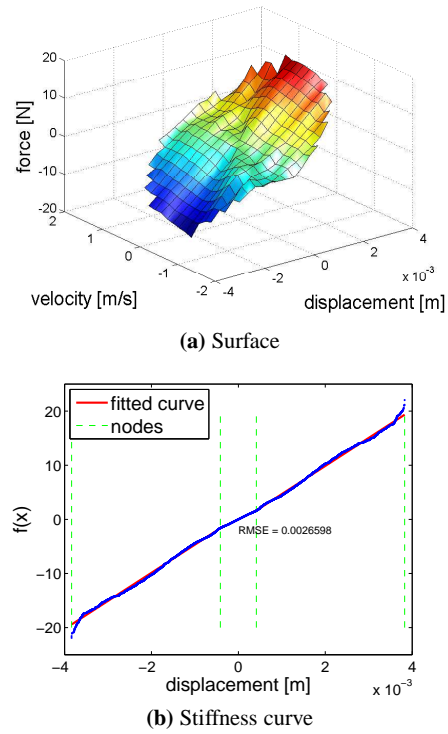


**(a)** Surface



**(b)** Stiffness curve

**Fig. 7:** Restoring force surface results

**Table 2:** Identified stiffness parameters for the symmetric gap

|  | $k_-$ | $k$ | $k_+$ |
|---|---|---|---|
| exact param. | 5318.6 | 3592.4 | 5318.6 |
| identified param. | 5196.5 | 3939.7 | 5188.3 |

**Table 3:** Identified gap size parameters for the symmetric gap

|  | $y_c$ | $y_c$ |
|---|---|---|
| exact param. | -0.0004 | 0.0004 |
| identified param. | -0.000414 | 0.000414 |

## 5 An industrial application: the IXV flap structure

Thanks to the numerical example, the method has been proved to be reliable as far as the identification of non-linear systems is concerned, therefore it can be applied to an industrial case in which a non-linearity showed up during the testing phase. It has to be underlined that the tests conducted on this structure were not meant for this purpose.

The application of this identification method to a real-life structure was successfully attempted in [9], where data coming from numerical simulations were used, and then applied on experimental data of a real satellite in [8]. Therefore the next section can be seen as an additional confirmation of the validity of the Restoring Force Surface method as a means of identifying nonlinear structures starting from the experimental data.

The structural element taken into account in this section is the flap of the Intermediate eXperimental Vehicle [18], which was successfully launched on 11 February 2015. The experimental data showed in the next sections and the FE model used for the numerical simulations were provided by Thales Alenia Space Italia (TAS-I), the project prime contractor. A detailed description of the flaps, together with the Flap Control System can be found in [19].

### 5.1 Experimental results.

The flap was tested on a shaker table (Fig. 8) under a sine-sweep excitation band-limited in the frequency range $5 - 100 \, Hz$, the sweep rate was set to $4 \, oct/min$ and the acceleration was enforced in the out of plane direction.



**Fig. 8:** Flap testing set-up (Courtesy of TAS-I)

Different levels of excitation were tested and the acceleration responses were measured and stored with sampling frequency of $6.5 \, kHz$. Since during structural tests the responses are usually stored as frequency domain data, the resulting time histories of some of them were not available.

The input excitations of the two tests taken into consideration are the first and the second shown in Fig. 9.

Looking at the frequency responses obtained from the tests (Fig. 10), it is clear that three modes participate to the response and this will negatively affect the identification results, as will be explained later.
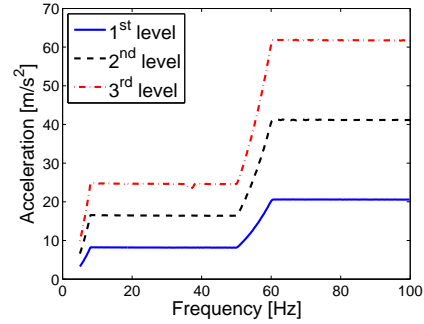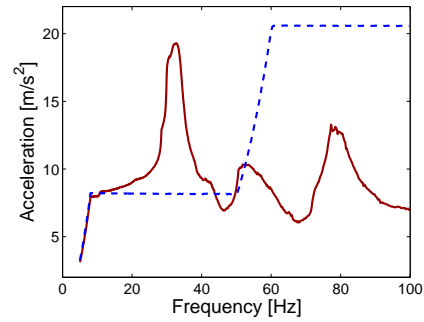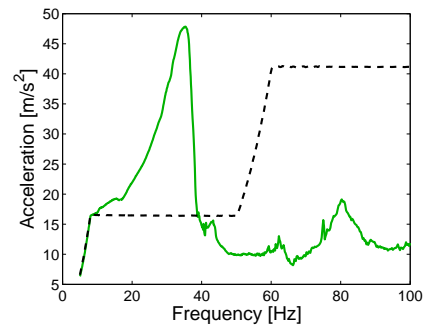


**Fig. 9:** Input excitations IXV test (Courtesy of TAS-I)



**(a)** Excitation level 1



**(b)** Excitation level 2

**Fig. 10:** Frequency responses at CoG from test (Courtesy of TAS-I)

The presence of the non-linearity is clearly visible when comparing the transmissibilities for the different excitation levels (Fig. 11), in fact, the resonance frequency shifts towards higher frequencies (from $32.63 \, Hz$ to $36.53 \, Hz$), therefore the non-linearity is expected to be of the hardening type.
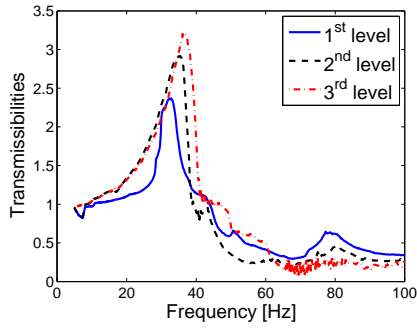
**Fig. 11:** Homogeneity test - IXV flap (Courtesy of TAS-I)

Being the tip the part that vibrates the most, and therefore the one that gives the highest evidence of the presence of the non-linearity, the first attempt implied the use of the acceleration measurement coming from the tip accelerometer. Unfortunately, looking at the response (Fig. 12) is clear that there is cross coupling between the modes and the contribution of the third mode (which corresponds, looking at the modeshapes, to the torsional mode) is far from being negligible. Moreover, the contribution of that mode could not be filtered out, otherwise all the harmonics generated by the non-linearity would have been lost. Since the Restoring Force Surface method is meant to deal with SDOF systems, this measurement had to be discarded.
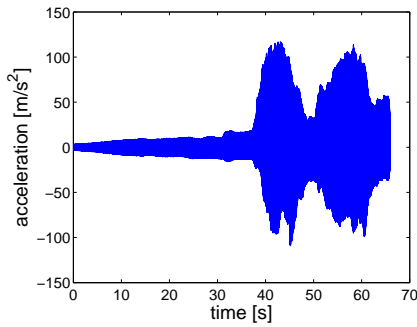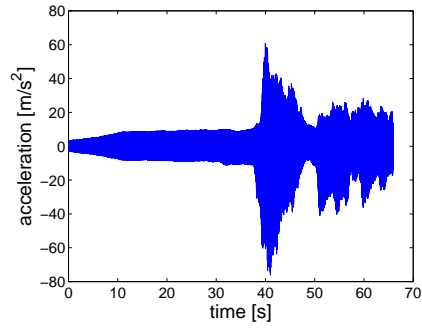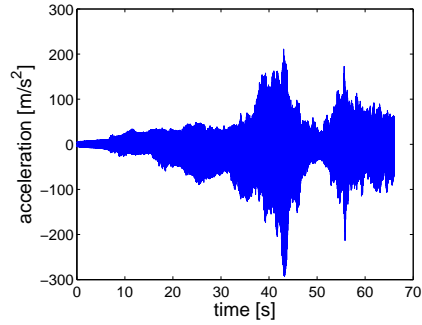


**Fig. 12:** Acceleration measured at the tip (Courtesy of TAS-I)

The second choice was the accelerometer placed at the centre of mass, which gave the time histories shown in Fig. 13. The contribution of the higher modes is still present (and can not be removed for the reason explained earlier), but the cross coupling is less than before. It has to be noted however, that the presence of other modes will negatively affect the identification results, because the structure does not behave exactly as a SDOF system.



**(a)** Excitation level 1



**(b)** Excitation level 2

**Fig. 13:** Acceleration measured at the CoG (Courtesy of TAS-I)

### 5.2 Parameters identification.

Since the excitation was given as enforced base acceleration, the formulation to be used for the restoring force computation had to be changed accordingly. The equation of motion became

$$m\ddot{y} + f(w_L, \dot{w}_L) = 0 \qquad (4)$$

where $m$ is the effective mass, $\ddot{y}$ is the absolute acceleration, $w_L = y - e_b$ and $\dot{w}_L$ are the displacement and the velocity relative to the substrate, respectively, whereas $e_b$ is the base displacement. The mode taken into account for the parameters identification is the first one.

To correctly scale the restoring force, the effective mass was needed and it was found to be equal to the $42.95\%$ of the total mass.

The Restoring Force Surface method was first applied to the data obtained from the first test (Fig. 13a). As can be seen from Fig. 14, the behaviour was not linear but, due to the contribution coming from the other modes, it was not possible to state without doubt that the distortions were caused by the non-linearity only. In addition, it was not possible to identify a clear non-linear trend comparable with one of the theoretical curves that represent the most common types of non-linearities.

By contrast, when applying the identification method to the data coming from the second test (Fig. 13b), the stiffness
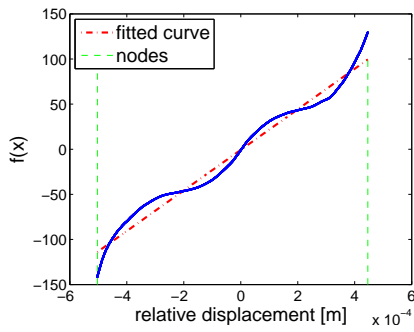
**Fig. 14:** Stiffness curve obtained from the data of the first test

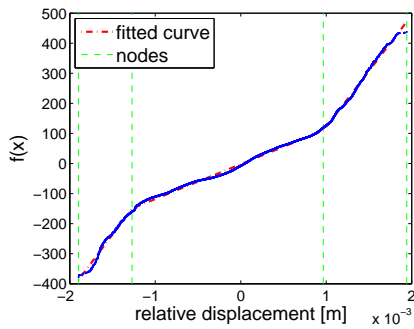curve clearly showed the piecewise linear trend (Fig. 15) typical of the free-play non-linearities.



**Fig. 15:** Stiffness curve obtained from the data of the second test

Due to the fact that it was not possible to rely on theoretical formulations to compute an estimate of the stiffness values, the identification process was focused on the determination of the gap size only. However, if the aim of the identification process is the update of the FE model, the free-play value is the only parameter needed to model the gap by means of the CGAP card. The identified free-play values are collected in Table 4.

**Table 4:** Identified free-play values

| $d_1$ [m] | $d_2$ [m] |
|-----------|-----------|
| -0.0013   | 0.0010    |

5.3 FE model updating.

Once the parameters which describe the non-linearity have been identified, the FE model can be updated in order to check its capability of predicting the behaviour of the flap for different load levels.

First of all, a linear transient analysis (SOL109) was run applying the first load level used in the test. The input excitation was applied to the structure as enforced acceleration by means of the Large Mass Method (the only available for the non-linear transient solution sequence SOL129). The out-of-plane response of the node corresponding to the accelerometer position during the test is plotted in Fig. 16.
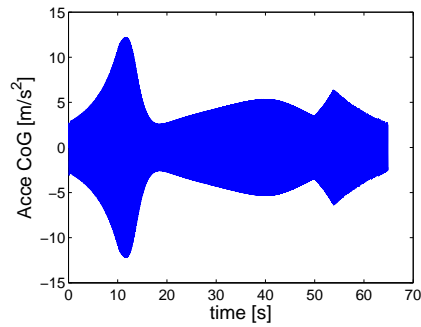


**Fig. 16:** Acceleration responses at CoG - linear transient

The gap location was identified to be at one of the hinge bearings, where it was meant to accomodate the distortions caused by thermal and pressure effects (further details of the flap design can be found in [19]). The gap was modelled at the hinge indicated in Fig. 17, in one direction only since only one set of measurements were used for the identification.
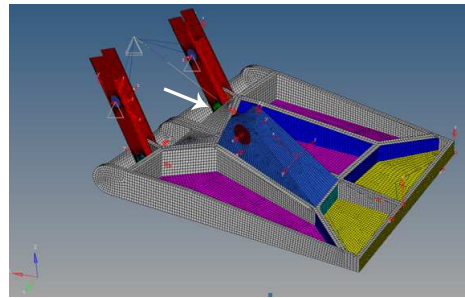


**Fig. 17:** Flap FE model (Courtesy of TAS-I)

The non-linear transient analysis has been run for both excitation levels and yields the results shown in Fig. 18. These responses seem to match the trend of the ones obtained from the test (Fig. 13), but for the spikes in the first few seconds of simulation, which were probably due to instabilities in the numerical solution caused by the structural damping definition by means of the PARAM,G and PARAM,W3 parameters. In fact, since non-linear transient analysis are direct solutions, the structural damping has to be defined at a certain frequency only (usually the system dominant frequency and indicated by the W3 value), which means that all

the frequencies before the values indicated by W3 will see a lower structural damping and thus the response will see a higher amplification (see Appendix B for more details).
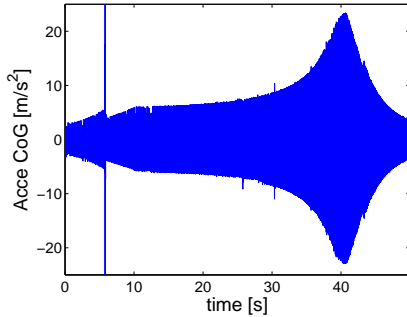


**(a)** Excitation level 1
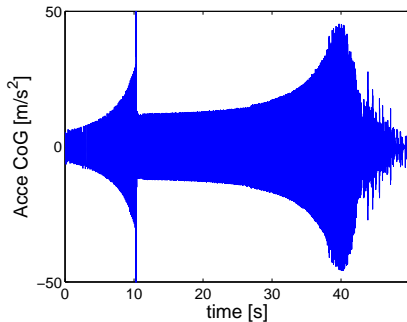


**(b)** Excitation level 2

**Fig. 18:** Acceleration responses at CoG in the presence of the gap

Nevertheless, the resonance is reached at the same time instant of the test and the *jump phenomenon* becomes more evident as the excitation level increases. However, the amplitude of the peak is not reproduced correctly, probably because the non-linearity present in the real system is more complex than the one that has been modelled. Looking at the frequency responses obtained by applying the Fourier transform to the time histories obtained from the Nastran simulations (Fig. 19), the effect of the non-linearity becomes even more visible and the hardening behaviour is reproduced correctly (the resonance frequency shifts towards higher frequencies). However, the responses show a lower amplitude if compared to the ones measured during the test (Fig. 10). An improvement in the non-linear behaviour could be obtained modelling the gap in more than one direction to try to better simulate the hinge behaviour.

## 6 Conclusions and future work

The study aimed at applying the Restoring Force Surface method to a real-life structure, the IXV flap, in such a way to characterize the non-linearity which showed up during the
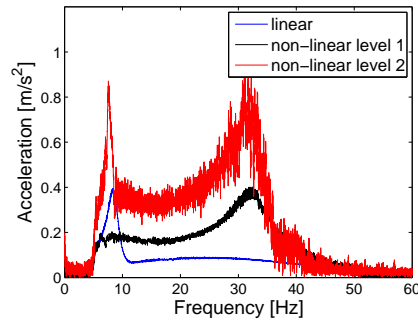


**Fig. 19:** Frequency responses calculated from transient responses

testing phase. Once the non-linear parameters were identified, they were used to update the FE model of the flap in order to make it capable of reproducing the flap behaviour for different load levels.

Before reaching this final step, the method implementation has been verified by means of a numerical example showing that the technique is an efficient tool as far as the identification of SDOF systems is concerned and that it is capable of providing powerful insight into the dynamics of these systems. However, since it requires the knowledge of acceleration, velocity and displacement signals, great effort has to be spent in data processing.

Since the study focused on stiffness non-linearities mainly, future work is needed to take into account the effect of the friction induced by the contact, which will lead to a more complex behaviour.

For what concerns the FE modelling of the non-linearities, the study focused on two different ways of modelling the free-play non-linearity. The first one relied on the definition of an element capable of simulating a point-to-point contact, whereas the second one implied the definition of non-linear load functions to generate direct forces from displacement functions. Both strategies have been successfully applied both in time and frequency domains on the simple case of the plate whereas in the case of the IXV flap the non-linearity has been modelled by means of the gap element in a non-linear transient analysis only.

A possible direction for future studies could be the modelling of the non-linearity in the frequency domain so that the numerical results could be directly compared to the test results, usually presented in the form of frequency responses and/or transmissibility functions.

For what concerns the FE model of the flap, future work should take into account the possibility of modelling the gap in more than one direction in order to reproduce a more realistic behaviour, also thanks to the possible inclusion of dry friction effects.

## A Velocity estimation via Kalman filter

As already mentioned in Section 1, one way to obtain the velocity estimate when both acceleration and displacement are measured is the use of a discrete Kalman filter. This approach was already presented in [3], but with a different formulation with respect to the one presented in this paper. An application of the methodology here presented can be found in [1].

An exhaustive introduction to the Kalman filter can be found in the original paper published by Kalman [20] and in Welch and Bishop paper [21], whereas here only the information needed to set-up the filter will be discussed.

The Kalman filter tries to estimate the state of a discrete-time process governed by Eq. (5)[2]

$$\mathbf{x_k} = \mathbf{A}\mathbf{x_{k-1}} + \mathbf{q_{k-1}} \tag{5a}$$
$$\mathbf{z_k} = \mathbf{H}\mathbf{x_k} + \mathbf{r_k} \tag{5b}$$

where $\mathbf{x}$ is the state vector, $\mathbf{A}$ is the state transition matrix, $\mathbf{z}$ is the vector of measurements and $\mathbf{H}$ is the observation matrix. The random variables $\mathbf{q_k}$ and $\mathbf{r_k}$ represent the process and measurement noise respectively and they are assumed to be independent of each other, white and with normal probability distributions given by

$$p(\mathbf{q}) \sim N(0, \mathbf{Q}) \tag{6}$$
$$p(\mathbf{r}) \sim N(0, \mathbf{R}) \tag{7}$$

where $\mathbf{Q}$ is the process noise covariance matrix, which serves the purpose of taking into account all the factors that influence the system and that are not know and/or modelled, and $\mathbf{R}$ is the measurement noise covariance matrix.

The state vector $\mathbf{x}$ and the matrix $\mathbf{A}$ can be written by considering the equations that describe the system, which are:

$$p_k = p_{k-1} + \Delta t v_{k-1} + \frac{\Delta t^2}{2} a_{k-1} \tag{8a}$$
$$v_k = v_{k-1} + \Delta t a_{k-1} \tag{8b}$$
$$a_k = a_{k-1}; \tag{8c}$$

where $p$, $v$ and $a$ represent position, velocity and acceleration respectively. Therefore, $\mathbf{x} = [p\ v\ a]^T$ and $\mathbf{A}$ takes the form:

$$\mathbf{A} = \begin{bmatrix} 1 & \Delta t & \dfrac{\Delta t^2}{2} \\ 0 & 1 & \Delta t \\ 0 & 0 & 1 \end{bmatrix} \tag{9}$$

Since the measured quantities are acceleration and displacement, the observation matrix $\mathbf{H}$ takes the form:

$$\mathbf{H} = \begin{bmatrix} 1 & 0 & 0 \\ 0 & 0 & 1 \end{bmatrix} \tag{10}$$

For what concerns the noise covariance matrices, $\mathbf{R}$ can be obtained by taking some off-line sample measurements and computing the variance of the measurement noise, whereas matrix $\mathbf{Q}$ needs a special attention. In fact, typically there is not the possibility to directly observe the process that needs to be estimated, therefore the determination of $\mathbf{Q}$ usually follows from an off-line tuning process, keeping in

mind that it must satisfy the properties of a covariance matrix, which means it must be symmetric and positive-semidefinite.

Since the effect of $\mathbf{Q}$ is to increase the uncertainty of the prediction, it is possible to define some guidelines for the choice of $\mathbf{Q}$:

– huge values (compared to $\mathbf{P}$, the error covariance) means that the model does not predict the process accurately enough, but if $\mathbf{Q}$ is too large, the filter will be too much influenced by the noise in the measurements
– low values of $\mathbf{Q}$ indicate confidence that any unknown noise term and/or modelling error is small, but the filter may become overconfident in its estimate of the state which could diverge from the actual solution

Now that all the elements have been defined, the discrete Kalman filter can be implemented as explained in [21].

To test its performance, the filter was applied to some measurements obtained from a test on a cantilever beam excited with a stepped-sine sequence band-limited in the $55 - 70\ Hz$ range. Both the acceleration and displacement responses (Fig. 20) were measured and the data were acquired with sampling frequency set to $200\ Hz$.



**(a)** Acceleration
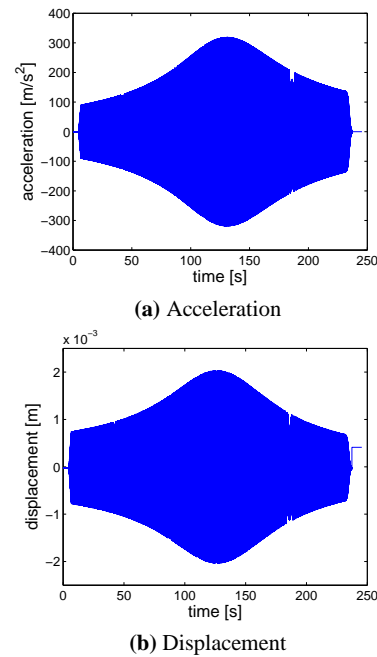


**(b)** Displacement

**Fig. 20:** Measured responses

In this case the process noise covariance matrix was the following

$$\mathbf{Q} = \begin{bmatrix} 2e6 & 5e7 & 0 \\ 5e7 & 8e9 & 5e3 \\ 0 & 5e3 & 2e6 \end{bmatrix} \tag{11}$$

To start the iteration, initial estimates are needed. For the case in hand, an initial state vector $\hat{\mathbf{x}}_0 = [0\ 0\ 0]^T$ has been chosen. Since the initial state is a guess, the starting covariance matrix $\mathbf{P_0}$ has been set to a large value. In fact, matrix $\mathbf{P}$ is an indicator of the variability of the state: if $\mathbf{P_k}$ is large, it means that the state is estimated to change a lot.

The velocity obtained applying the Kalman filter has been compared to the one obtained by integration and filtering (by means of a fourth-order Butterworth filter with cut-off frequency set at $5\ Hz$) of

---

[2] In the original equations presented by Kalman in [20] there was also a term $\mathbf{B}u$, which is added to Eq. (5a) and represents the input to the system. This term is here omitted because there is no input term in Eq. (8)

the accelerometer data. The comparison is shown in Fig. 21, a magnification of the signals is shown in Fig. 22. As can be seen, they are virtually identical, which means both methods are valid in terms of performance. The drawback which limits the use of the Kalman filter is related to the need of measuring both acceleration and displacement, which is not something that is usually done during tests. In addition, when integrating and filtering the acceleration data, the only parameter that has to be defined is the filter cut-off frequency, which has a more intuitive meaning than the process noise covariance in the Kalman filter.
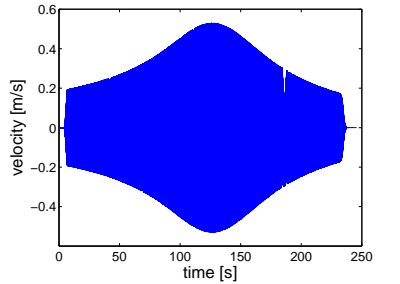


**(a)** Integrated and filtered from acceleration
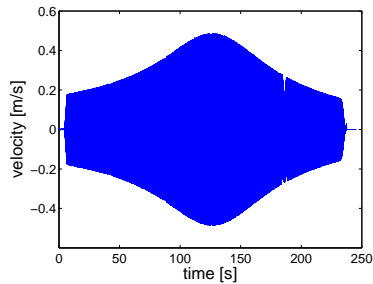


**(b)** Estimated using Kalman filter

**Fig. 21:** Comparison between integrated and estimated velocity
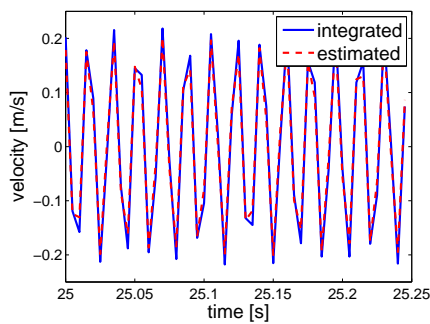


**Fig. 22:** Magnification of the curves in Fig. 21

## B Damping definition in direct solutions

Damping, in dynamic analysis, is a mathematical approximation to account for energy dissipation and therefore for reduction in the structural response, which, in the physical system, is due to the presence of internal friction. The type of damping taken into account in all the simulations performed during this study is the structural damping. Structural damping can be defined in different ways depending on the type of solution sequence used. Being the SOL129 a direct transient solution, the damping had to be defined by means of the PARAM,G and the PARAM,W3 parameters, where G indicates the damping value (at resonance $G = 2\xi$ where $\xi = \dfrac{c}{c_{cr}}$ is the damping ratio) and W3 indicates the frequency at which the damping is defined. This means that the damping is correct only for the frequency selected by the PARAM,W3, which is usually chosen equal to the system dominant frequency. Since the structural damping force is constant with respect to the forcing frequency, every frequency lower than W3 sees a lower damping and every frequency greater than W3 gets more damping.

The effects of the different choices of the PARAM,W3 can be seen comparing Fig. 24 to Fig. 23, where the W3 parameter has been set to $50.26 \ rad/s$ ($\simeq 8 \ Hz$) in the first figure and to $194.78 \ rad/s$ ($\simeq 31 \ Hz$) in the second (the frequencies selected to compute the parameter are the resonance frequencies of the structure with and without the gap). The choice of W3 greatly affects the simulation results, as can be seen comparing Fig. 23 and Fig. 24. In fact, in Fig. 23 the lower frequencies are enhanced, thus showing a response amplitude much greater than the one in Fig. 24, on the contrary, in Fig. 24 the higher frequencies are more damped, thus the response has a lower amplitude. The spikes visible in Fig. 18 come from the contribution of the low frequency mode also visible in Fig. 23, since in both analyses the dominant frequency has been chosen equal to $194.78 \ rad/s$ ($\simeq 31 \ Hz$).
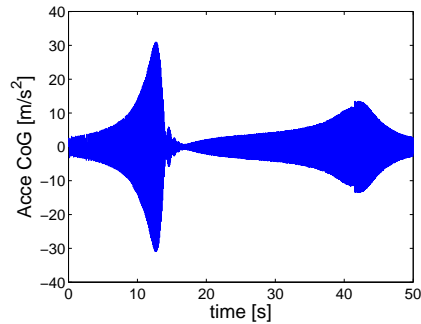


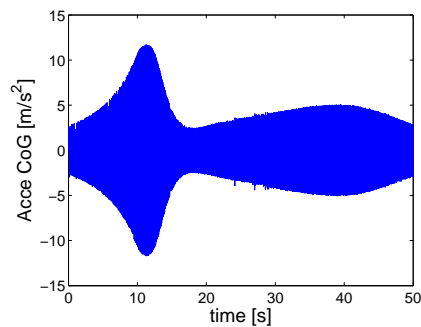**Fig. 23:** Time response obtained for W3 $= 194.78 \ rad/s$



**Fig. 24:** Time response obtained for W3 $= 50.26 \ rad/s$

# References

1. S.O.Vismara, *Non-linear spacecraft component parameters identification based on experimental results and finite element model updating*, Master of Science thesis, (2015)
2. G. Kerschen, K. Worden, A.F. Vakakis, J.C. Golinval, *Past, present and future of nonlinear system identification in structural dynamics*, Mechanical Systems and Signal Processing 20, pp.505-592, (2006)
3. E.F. Crawley, K.J. O'Donnel, *Identification of non-linear system parameters in joints using the Force-State Mapping Technique*, MIT SSL Report, (1985)
4. K. Worden, G.R. Tomlinson, *Nonlinearity in structural dynamics: detection, identification and modelling*, Institute of Physics Publishing, (2001)
5. M.S. Allen, H. Sumali & D.S. Epp, *Restoring force surface analysis of nonlinear vibration data from micro-cantilever beams*, Proceedings of IMECE, Chicago, Illinois (2006)
6. M.Haroon, D.E. Adams, Y.W. Luk, A.A. Ferri, *A time and frequency domain approach for identifying nonlinear mechanical system models in the absence of an input measurement*, Journal of Sound and Vibration 283, pp.1137-1155, (2005)
7. G. Kerschen, J.C. Golinval, K. Worden, *Theoretical and experimental identification of a non-linear beam*, Journal of Sound and Vibration 244, pp.597-613, (2001)
8. J.P. Noel, L. Renson, G. Kerschen, *Complex dynamics of a nonlinear aerospace structure: experimental identification and modal interactions*, Journal of Sound and Vibration 333, pp.2588-2607, (2014)
9. J.P. Noel, G. Kerschen, A. Newerla, *Application of the Restoring Force Surface Method to a Real-life Spacecraft Structure*, Topics in Nonlinear dynamics, Volume 3, Proceedings of the 30th IMAC, A Conference on Structural Dynamics, (2012)
10. G. Kerschen, L. Soula, J.B. Vergniaud, A. Newerla, *Assessment of Nonlinear System Identification Methods using the SmallSat Spacecraft Structure*, Advanced Aerospace Applications, Volume 1, Proceedings of the 29th IMAC, A Conference on Structural Dynamics, (2011)
11. J.G.T. Ribeiro, J.L.F. Freire, J.T.P. de Castro, *Some comments on digital integration to measure displacements using accelerometers*, Shock and Vibration Digest, Volume 32, p.52 (2000)
12. J.G.T. Ribeiro, J.L.F. Freire, J.T.P. de Castro, *New improvements in the digital double integration filtering method to measure displacements using accelerometers*, Proceedings of the International Modal Analysis Conference - IMAC, Volume 1, pp.538-542 (2001)
13. Steven W. Smith, *The Scientist and Engineer's Guide to Digital Signal Processing*, Second edition, California Technical Publishing
14. R.G. Lyons, *Understanding digital signal processing*, Second edition, Prentice Hall
15. MSC Nastran 2013, *Dynamic Analysis User's Guide*
16. MSC Nastran 2013.1, *Quick Reference Guide*
17. K. Vanhoenacker, J. Schoukens, J. Swevers, D. Vaes, *Summary and comparing overview of techniques for the detection of non-linear distortions*, Proceedings of ISMA, Volume 3, (2002)
18. E. Zaccagnino, G. Malucchi, V. Marco, A. Drocco, S. Dussy and J.P. Préaud, *Intermediate eXperimental Vechicle (IXV), the ESA re-entry demonstrator*, AIAA Guidance, Navigation and Control Conference, Portland, Oregon, (2011)
19. D. Verhoeven, D. Renté, *Locking mechanism for the IXV re-entry demonstrator flap control system*, 14th European Space Mechanisms and Tribology Symposium - ASMATS 2011, Constance, Germany, (2011)
20. R.E. Kalman, *A new approach to linear filtering and prediction problems*, Transaction of the ASME - Journal of Basic Engineering, Volume 82, pp.35-45 (1960)
21. G. Welch, G. Bishop, *An introduction to the Kalman filter*, (2006)